

Deep Activity Model: A Generative Deep Learning Approach for Human Mobility Pattern Synthesis

Xishun Liao¹, Qinhua Jiang¹, Brian Yueshuai He², Yifan Liu¹, Chenchen Kuai³, Jiaqi Ma^{1*}

Abstract—Human mobility plays a crucial role in transportation, urban planning, and public health. Advances in deep learning and the availability of diverse mobility data have transformed mobility modeling. However, existing deep learning models often focus on spatio-temporal patterns and struggle to capture the semantic interdependencies among activities, while also being limited by specific data sources. These challenges reduce their realism and adaptability. Traditional activity-based models (ABMs) face issues as well, relying on rigid assumptions and requiring extensive data, making them costly and difficult to adapt to new regions, especially those with limited conventional travel data. To address these limitations, we develop a novel generative deep learning approach for human mobility modeling and synthesis that incorporates both activity patterns and location trajectories using open-source data. The model can be fine-tuned with local data, allowing it to adapt to and accurately represent mobility patterns across diverse regions. The model is evaluated on a nationwide dataset of the United States, where it demonstrates superior performance in generating activity-location chains that closely follow ground truth distributions. Further tests using state- or city-specific datasets from California, Washington, and Mexico City confirm its transferability. This innovative approach offers substantial potential to advance mobility modeling research, particularly in generating synthetic human mobility data. This can provide urban planners and policymakers with enhanced tools for simulating mobility in diverse regions and better informing decisions related to transportation, urban development, and public health.

Index Terms—Mobility trajectory generation, travel behavior, household travel survey, synthetic dataset

I. INTRODUCTION

A. Motivation

Understanding and synthesizing human mobility patterns has gained considerable importance as population growth, increasingly complex travel behaviors and diverse societal needs reshape modern transportation systems [1]. Human mobility impacts numerous facets of contemporary life, including traffic management, air quality, energy consumption, and public health. The COVID-19 pandemic, for instance, substantially altered mobility behaviors due to widespread shifts to remote work and decreased travel demand [2]–[5]. Additional factors affecting human mobility include traffic congestion and safety [6]–[8], citizen well-being [9], events [10], air pollution [11], and energy and water

consumption [12]. Consequently, modeling human mobility has garnered substantial research interest due to its relevance in addressing these critical issues.

Traditional models of human mobility include Activity-Based Models (ABMs), developed in the late 1990s [13]. ABMs simulate the sequence of individual activities and predict interdependent activity choices, making them popular with Metropolitan Planning Organizations in the U.S. [14]. For instance, ABM is used to predict activity patterns and travel demand for Southern California, a region with about 26 million population [15], [16]. However, ABMs have significant limitations: data collection, model development, and calibration are costly and time-consuming; their complexity leads to high computational demands; and they rely on numerous assumptions, limiting their adaptability to other regions.

Data-driven approaches, including deep learning (DL) and generative algorithms, offer promising alternatives to address the limitations of ABMs in replicating human mobility trajectories. These methods can accurately mimic real-world patterns, aligning closely with observed data [17]–[20]. Prior research has focused on spatial (e.g., travel distance [21], preferred locations [22]) and temporal attributes (e.g., activity schedules [23]). Additionally, over 90% of human mobility patterns exhibit recurring motifs, indicating that pre-trained models can be adapted to various regions [24], [25].

Despite their advantages, current DL models often rely on specialized mobility data sources like GPS, social media, and communication records [21], [26], [27]. These sources differ in format and availability, making cross-dataset and regional adaptation challenging. Additionally, access to such data can be costly, limited, and difficult, reducing model flexibility. Many models focus solely on spatial-temporal trajectories, overlooking the semantic relationships between activities and socio-demographic factors. These limitations highlight the need for adaptable models that can capture the complex interdependencies of activities, locations, and personal attributes.

B. Objective and Study Scope

Objective: In this paper, we aim to address the limitations of existing ABMs and data-driven mobility methods by introducing a novel generative deep learning model, referred to as the Deep Activity model. Our primary objective is to synthesize human mobility patterns only based on agent profiles and to reveal fundamental and generic mobility trends within a given region. We interpret human mobility patterns as chains of activities (i.e., travel demand) and locations that individuals visit, influenced by socio-demographic factors and environmental conditions. Unlike previous approaches that focus on

¹ Xishun Liao, Qinhua Jiang, Yifan Liu, and Jiaqi Ma are with UCLA Mobility Lab at University of Los Angeles, Los Angeles, CA 90095, USA.
*Corresponding author: Jiaqi Ma, jiaqima@ucla.edu

² Brian Yueshuai He is with Civil and Environmental Engineering Department at University of Louisville, Louisville, Kentucky, 40208, USA

³ Chenchen Kuai is with Civil and Environmental Engineering Department at Texas A&M University, College Station, Texas, 77840, USA

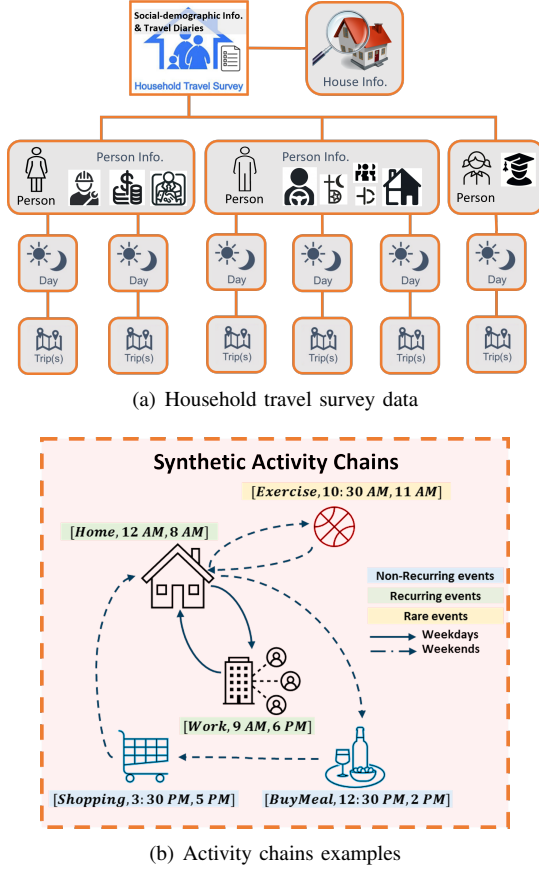


Fig. 1. Model human mobility pattern using HTS data. (a) HTS data includes information about each household member's socio-demographics, household characteristics, and daily non-commercial travel across all modes, including details about travelers, their households, and vehicles [28]. (b) Typical weekday and weekend activity chains in HTS.

predicting the next point of interest (POI) or activity based on historical data, our model emphasizes generation, producing synthetic yet realistic human mobility patterns without relying previous information.

Study Scope: The scope of this research is centered on modeling human mobility at both the demand and trajectory levels. Our Deep Activity model is derived from trip diaries available in household travel survey (HTS) data (Fig.1 (a)). We utilize the concept of an "activity chain" (Fig.1 (b)), which represents a one-day sequence of activities for individuals. Leveraging regional population information, the Deep Activity model generates realistic and varied activity chains. With assigning specific locations to each activity in the chain, our proposed method effectively captures the underlying human mobility patterns of the target region. Furthermore, the model can be fine-tuned for specific regions, capturing unique patterns in California, the Puget Sound region (Washington state), and Mexico City.

C. Contributions

With such synthesis capability, the automatic generation of transportation system simulation models becomes much more feasible. This addresses the significant challenge of the extremely high costs and labor-intensive nature of hand-crafted models that have persisted for a long time. More

implications include facilitating location choice models and urban planning models by integrating the Deep Activity model. This paper sets the foundation for human mobility synthesis, enabling the automatic generation of data for new regions and significantly advancing the field of transportation modeling. Our key contributions include:

- We are the first to define the human mobility pattern synthesis problem, encompassing both travel demand generation and travel trajectory creation, while ensuring privacy by utilizing aggregated survey data instead of individual-level trajectory data. Additionally, we introduce new performance metrics for effective evaluation.
- We propose a deep learning model to generate synthetic human mobility data based on socio-demographic information and household characteristics. The model is transferable and can be fine-tuned with local data, making it suitable for data-limited regions. By leveraging HTS data, an effective loss function, and optimizing input construction, even a vanilla transformer model proves highly effective in addressing this complex problem. Additionally, we integrate mobility generation with activity location assignment, validating the model's performance by embedding generative travel demand into a large-scale simulation network.
- We explicitly model the interdependencies among activities of household members, investigating how decisions made by one member influence others, thus capturing household-level mobility dynamics.
- We explore a standard technique for multivariate, multi-objective data balancing to process the ubiquitous HTS data. This pioneering approach enhances the applicability of HTS data in deep learning models for human mobility studies, providing significant benefits to the transportation modeling and planning community.

II. RELATED WORK

Human mobility has gained attention recently due to increased data availability, computing advancements, and AI techniques. Research in this field focuses on two main tasks: generation and prediction [29]. Generative models aim to create realistic human trajectories, replicating real-world mobility flows, while prediction models forecast individual movements or crowd flows based on historical data [30]–[32]. This paper focuses on generative models, specifically addressing the challenge of generating realistic activity chains in human mobility patterns.

Transportation Models. ABMs are the state-of-the-practice model to generate human activity patterns. An ABM is a type of modeling approach used in transportation planning and urban studies to predict and analyze individual activity patterns and travel behavior. ABMs aim to understand and simulate how people make decisions about their daily activities, such as work, shopping, education, recreation, and other social and personal activities, and how these activities influence their travel choices and travel patterns. Bowman and Ben-Akiva [33] proposed an ABM prototype to predict individual activity and travel schedule based on discrete choice models

and forecasted the travel demand of the Boston metropolitan area. Goulias et al. [34] developed SimAGENT, an ABM to simulate activity and travel patterns in Southern California. SimAGENT comprises five components: a population synthesizer, socioeconomic micro-simulator, land use and transportation systems, daily activity-travel micro-simulator, and transportation simulation [35]. However, the development of ABMs requires extensive data collection, making them expensive and resource-intensive. Additionally, their reliance on localized data limits their adaptability to different regions, which restricts their broader applicability.

Model-Based Data Driven Methods. Data-driven models offer an alternative approach for activity generation problems. The Exploration and Preferential Return (EPR) model, a stochastic method, simulates human mobility by balancing exploration of new locations with returns to previously visited ones [36]. In the EPR model, individuals move through a spatial environment, making decisions influenced by location popularity and distance. The model considers the balance between exploration and preferential return and evolves over time. Enhancements like TimeGeo by Jiang et al. [37] add temporal choices, such as home-based tour number, dwell rate, and burst rate, along with a hierarchical multiplicative cascade method to measure generated trips and land use. These improvements bypass HTS data limitations by offering a flexible, data-driven framework. However, model-based data-driven methods often require prior expert knowledge, and their simple implementation mechanisms may constrain realism [38].

Deep Learning Approaches. Multiple DL models have been used to model human mobility and generate human activities and trajectories, including fully connected networks, recurrent neural networks (RNNs), attention mechanisms, convolutional neural networks (CNNs), and generative models such as Generative Adversarial Networks (GANs) and Diffusion Models. For a detailed review, see Luca et al. [29]. The limitations of model-based, data-driven methods can be addressed by generative models, as they can simultaneously incorporate various aspects of human trajectories (e.g., spatial and temporal features) and capture complex, non-linear relationships in the data. GANs and diffusion models, in particular, are well-suited for modeling complex data structures like detailed trajectory data due to their ability to learn intricate movement patterns. However, these models require large amounts of high-quality data to train effectively [39], which poses challenges when dealing with simpler data formats, such as survey data, where individuals have fewer activities and locations. However, the performance of DL models heavily depends on the quantity and quality of data, and they are constrained by the fact that human mobility data is often expensive or difficult to access (e.g., requiring Non-Disclosure Agreements). Thus, exploring the potential of DL models to synthesize human mobility patterns using ubiquitous and open-source data is essential.

III. PROBLEM FORMULATION

One of the fundamental principles of ABM is that "the demand for travel is derived from the demand for activities" [33].

This principle highlights the nature of human mobility, where activities form the foundation of human trajectories. In this study, the concept of an "activity chain" is used to describe the structure of these trajectories, and the human mobility of a region can be represented by the activity chains of its population.

We denote i for an agent. An activity chain for the agent i is a time-ordered sequence $A_i = \{A_{1,i}, A_{2,i}, \dots, A_{n,i}\}$, where $A_{n,i} = [T_{n,i}, S_{n,i}, E_{n,i}]$ represents the n -th activity conducted by agent i . Here, $T_{n,i}$ is the activity type of $A_{n,i}$. $S_{n,i}$ and $E_{n,i}$ stand for start time and end time of $A_{n,i}$, respectively. Then the mobility trajectory can be expressed as $Traj_i = \{(A_{1,i}, Z_{1,i}), \dots, (A_{n,i}, Z_{n,i})\}$, where $Z_{n,i}$ denotes the zone-level location where the $A_{n,i}$ occurs. A generative model M can generate activity chains A_i for each individual i , given socio-demographic attributes of the target agent and other household members, $D_{k,i} = \{d_{1,i}, d_{2,i}, \dots, d_{K,i}\}$, where $d_{K,i}$ represents the k -th socio-demographic attributes.

IV. DATASET

A. Household Travel Survey

To generate the activity chain for each individual in the region of interest, we rely on data collected through the HTS, following a standard format across different regions, as introduced in Fig. 1(a). In the US, this survey is usually conducted by federal agencies or state agencies to gather detailed information about people's travel behaviors. The Federal Highway Administration (FHWA) administered the National Household Travel Survey (NHTS) for the United States [40]. To uncover regional activity patterns, many states also conducted statewide HTS [41]–[44]. This travel-diary data source is also widely available in many countries as government agencies need such data for various purposes of public resource management. Unlike trajectory data, which includes detailed location traces that could potentially identify individuals when combined with demographic information, HTS data focuses on summarized activity patterns and aggregated travel behaviors, which helps to mitigate privacy risks.

Building on this standardized HTS data, the Deep Activity model can be easily trained and transferred to other regions. In this study, the generic model is developed using the 2017 NHTS to enhance adaptability across regions, leveraging its large dataset of over 129,600 US households, which includes demographics, activity patterns, and travel behaviors for each household member. As presented in TABLE I, the activity types in NHTS are aggregated to 15 types based on the locations of activities. For instance, regular home activities and work from home are grouped as the home activity. Besides NHTS, the 2010–2012 California Household Travel Survey [42] (collected from 42,500 households), the 2017 Puget Sound Regional Travel Study [43] (collected from 3,285 households), and the 2017 Origin-Destination Survey across the Mexico City Metropolitan Area [44] (collected from 66,625 housing units) are adopted in this study for transferability exploration.

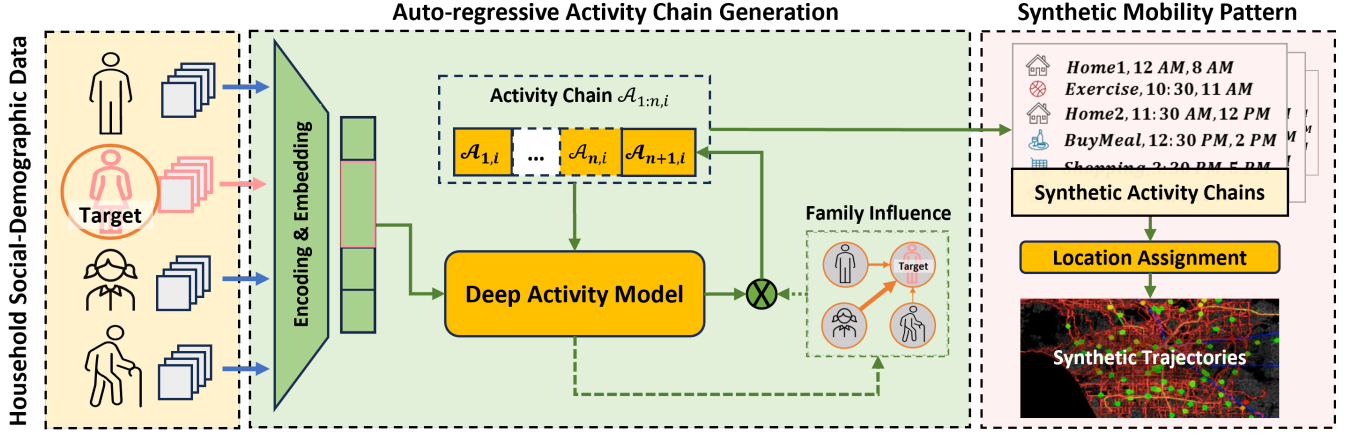


Fig. 2. Workflow of activity chain generation. Given the synthetic socio-demographic information and household characteristics of each agent, the model auto-regressively synthesizes the agent’s activity chain and the location of each activity.

TABLE I
ACTIVITY CATEGORY CODE AND THEIR CORRESPONDING DESCRIPTIONS
FROM 2017 NHTS

1	Home	2	Work	3	School
4	Care giving	5	Buy goods	6	Buy services
7	Buy meals	8	General errands	9	Recreational
10	Exercise	11	Visit friends	12	Health care
13	Religious	14	Something else	15	Drop off/Pick up

B. SCAG ABM Data

In addition to the travel survey data, we utilize synthetic mobility data, specifically the SCAG ABM data [45], for this study. The SCAG ABM dataset represents simulated human mobility patterns, providing detailed synthetic single-day activity diaries across six counties in Southern California, encompassing a population of over 19 million. The model captures 24-hour travel demand patterns at a 15-minute temporal resolution, including start and end times, types of activities, and zonal-level locations for each individual agent.

One notable advantage of the SCAG ABM data is the inclusion of zonal-level location data for each simulated activity. These zones, known as Transportation Analysis Zones (TAZs), contain demographic and spatial information about the residents and destinations within each zone, serving as both origins and destinations of trips. The use of this data significantly enhances our ability to validate the spatial-temporal performance of the mobility patterns generated by the model proposed in this study, providing a robust framework for further analysis and validation. In this study, we select Los Angeles (LA) County, which contains 5,967 TAZs, as the target area for validation.

C. Data Preparation

The first step in training the model involves preparing the agent information and activity chain pairs, which includes selecting relevant features for the agent information and encoding the activity chain data.

According to ABM, **socioeconomic and demographic attributes** significantly influence individual activity patterns and travel choices. In the context of the activity generation model,

the function of these attributes is similar to a prompt (as in the language model), determining the start of activity sequence generation and influencing the entire sequence generation process. These attributes include typical individual characteristics, such as gender, race, age, employment status, and job category, capturing personal and professional demographics. Education level and student status provide insights into the academic background and current academic involvement.

Household-related attributes such as the number of persons, relationships within the household, home ownership, and household size are also considered for their impact on daily routines and mobility. The number of vehicles owned, workers in the household, and the household employed count are indicative of transportation needs and capabilities. Household income level, along with the percentage of renter-occupied housing in the household’s location, offers a socioeconomic perspective.

Additionally, **zonal attributes**, including the population density, housing units, and the classification of the residence type as rural or urban, provide a geographical context. Finally, the life cycle stage of the household is included as it reflects the evolving needs and behaviors of individuals over time. These demographic features collectively offer a comprehensive description of an individual’s background. Finally, there are 13 personal attributes, 13 household shared attributes, in total 26 attributes selected to describe one individual. In conclusion, the personal and household features used for the model are presented in Table II.

The attribute data, originally in text or label format, is transformed into categorical data. Not everyone answers all the privacy-related questions in the survey, so for any attributes left blank or marked as ‘not responded’ in the NHTS, we used a dummy number for encoding. The continuous activity start and end times are encoded with segmenting a 24-hour day into 96 intervals, each lasting 15 minutes, and numerically encoded from 1 to 96 to represent the time slots.

Regarding the **SCAG ABM dataset**, we sample subsets from the overall population of 10 million individuals for the purposes of model transfer learning and validation. Specifically, we prepare two subsets: a smaller sample of 100,000

individuals, which is used for model transfer learning, and a larger sample of approximately 1 million individuals, employed to assess the scalability of the model trained on the smaller subset to a larger population. The activity types in the SCAG ABM data are mapped to correspond to 15 categories consistent with the NHTS data, and the time variables are similarly encoded into 96 time slots, following the same procedure used for the NHTS data.

TABLE II
SOCIO-DEMOGRAPHIC ATTRIBUTES FROM HTS DATASET

Attribute Name	
Driver's License Status	Number of Workdays
Education Level	Job Category
Gender	Age
Racial/Ethnic Identity	Weekly Transit Usage
Household Role	Household Income
Current School Grade Level	Household Size
Employment Location Type	Household Vehicles
Number of Jobs	Home Ownership Status
Employment Status	Household Students
Household Licensed Drivers	Household Life Cycle Stage
Household Employed Members	Type of Residence
Housing Status	Housing Density
Population Density	Renter-Occupied Housing Ratio

V. METHODOLOGY

The workflow for generating activity chains for an individual using our Deep Activity model is illustrated in Fig. 2. The process begins with household socio-demographic data, which includes information about the target person and any family members. The Deep Activity model captures the influence of household members on the target person and ensures that the generated activity chain reflects real-world interdependencies. The model then auto-regressively generates a sequence of activities, forming the target person's activity chain A_i . Finally, location is assigned for each activity in A_i , completing the synthetic mobility trajectory generation.

A. Model Architectures

To generate an activity chain, comprising activity types alongside their corresponding start and end times, based on the demographic attributes of individuals. The structure of the activity chain generation problem is analogous to text generation tasks tackled by language models. Just as words in a sentence follow a logical sequence based on context, activities in a person's daily routine are sequentially dependent on preceding activities and time constraints. Hence, a model based on Transformer [46] is developed and trained for the activity chain generation task, as shown in Fig. 3.

Data structure design. To analyze the influence of household members and previous activities on the target person's decision, we developed an innovative data concatenation strategy. This approach combines embedded social-demographic data, data of other household members, and embedded activity data within the time domain. To standardize dimensions across these diverse data sets, we integrated fully connected layers and employed learnable delimiters <SEP> for separation. Fig. 3(a) illustrates this process for a household with five members,

demonstrating how the data is transformed into a comprehensive feature vector. This vector subsequently serves as input for the network's deeper layers, enabling more nuanced analysis. Our model is designed to accommodate households of up to five members, a decision informed by statistical analysis of the NHTS dataset, which reveals that 95% of households do not exceed this size.

Feature Embedding. We employ embedding layers to map each categorical variable into a continuous space, utilizing the Embedding function [47], which can be optimized through backpropagation. To ensure an accurate representation of categories, we created a distinct embedding layer for each categorical attribute. Formally, for a categorical feature c with N unique categories, the embedding function is defined as: $E_c : 1, 2, \dots, N \rightarrow R^d$, where d represents the dimension of the embedding space for that feature. The optimal value of d was determined through validation performance.

As illustrated in Fig. 3 (a), the embedding layer processes the activity chain data, represented by a tensor with dimensions (5, t, n), where these dimensions correspond to features, time, and batch size, respectively. Additionally, another embedding layer handles the target individual's social-demographic data, shaped as (26, 1, n), and the data pertaining to the target person and other household members. These diverse data sets are then seamlessly combined, utilizing five <SEP> delimiters to maintain a clear separation between different data types.

Network structure design. The network structure integrates a Transformer encoder-decoder architecture. As shown in Fig. 3 (b), the Transformer encoder receives combined embeddings of personal and household information, and previous activities, along with padding masks to ignore irrelevant parts and causal masks to maintain the autoregressive nature of the sequence prediction. The decoder then takes the combined activity sequence and the output (memory) from encoder as additional context. By processing the entire context in the encoder and focusing on the next activity prediction in the decoder, the model captures complex dependencies and interactions. This approach simultaneously considers personal, household, and previous activity influences on the target person's next activity decision, improving prediction accuracy and providing a deeper understanding of the factors driving activity choices. Next, positional encoding are added to both encoder and decoder inputs to retain temporal information. Finally, the model generates predictions for the activity type $T_{n,i}$, start time $S_{n,i}$, and end time $E_{n,i}$, forming the next activity. The prediction process continues until either the activity marked as the end-of-the-sentence (EOS) is predicted, or the chain reaches the maximum length, at which point the prediction terminates.

B. Loss functions

Predicting activity type is a classification task. Because the day was segmented into 96 intervals, each lasting 15 minutes, as described in Appendix B, predicting start and end times is also a classification task. **Cross-entropy loss**, $\mathcal{L}_{CE}(\mathbf{y}, \hat{\mathbf{y}}) = -\sum_i y_i \log(\hat{y}_i)$, is commonly used to measure the discrepancy between predicted probabilities and actual

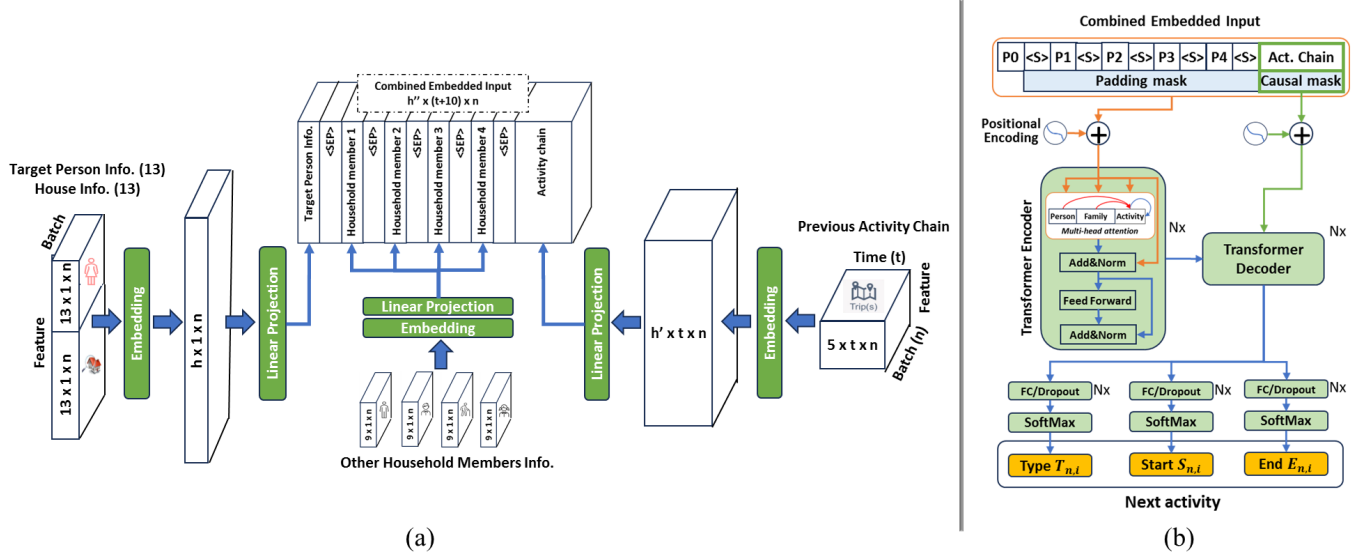


Fig. 3. Deep Activity model architecture. (a) Input data construction. (b) Transformer-based network architecture with well-designed data injection.

outcomes and is the first loss term to minimize activity mismatch. However, given the uncertainty of human activity, time prediction should not be overly strict but rather should allow for a certain level of deviation. Therefore, we incorporate a custom loss function that includes soft labels to allow the prediction results to deviate within a small window, enhancing the flexibility and robustness for start and end time prediction.

Soft label loss L_s . Soft label loss is calculated in two steps: 1) generate soft labels. 2) calculate the soft cross entropy loss. First, soft label matrix (S) of dimension $N \times C$ are generated by assigning higher weights to the true class and lower weights to adjacent classes. C denotes the number of activity class, and N is the batch size. For each true label step y_i , $S_{i,y_i} = w_m$, $S_{i,y_i \pm s} = w_s$ for $s \in [1, n_s]$, where w_m (set to 1) and w_s (set to 0.1) are the main and side weights, respectively, and n_s is the number of allowance deviation side steps.

Then the soft label cross entropy loss is computed as:

$$L_s = \frac{1}{N} \sum_{i=1}^N \left(- \sum_{j=1}^C S_{i,j} \log (P_{i,j} + \epsilon) \right), P_{i,j} = \frac{e^{Z_{i,j}}}{\sum_{k=1}^C e^{Z_{i,k}}} \quad (1)$$

where Z is the predicted result; $P_{i,j}$ represents the probability that the i -th sample in batch N belongs to the j -th class, as predicted by the model; ϵ is a small constant added to prevent the logarithm of zero.

Additionally, to guarantee that the generated sequence of activities adheres to a logical chronological order, two specialized time penalty losses, i.e., **temporal order loss (L_o)** and **sequential timing loss (L_{seq})**, are incorporated. These losses ensure that the predicted end time of an activity does not precede its start time and that the end time of a preceding activity does not exceed the start time of the subsequent activity.

$$L_o = \frac{1}{N} \sum_{i=1}^N \max (0, t_{i-1}^{\text{end}} - t_i^{\text{start}}), \quad (2)$$

$$L_{seq} = \frac{1}{N} \sum_{i=1}^N \max (0, t_i^{\text{start}} - t_i^{\text{end}})$$

where t_{i-1}^{end} denotes activity end time at $i-1$ step, and t_i^{start} means activity start time at i step.

Our final loss L combines five loss terms as below:

$$L = w_1 \cdot L_{CE}(T, \hat{T}) + w_2 \cdot L_s(S, \hat{S}) + w_3 \cdot L_s(E, \hat{E}) + w_4 \cdot L_o + w_5 \cdot L_{seq} \quad (3)$$

C. Data Balancing

To create a fair and representative training dataset for model development, data balancing is essential to address the imbalances in HTS data. Most people follow similar activity patterns [24], [25], which can overshadow less common activities and lead to biased models favoring the majority class. To address this, we developed a multivariate, multi-objective data balancing technique for curating the HTS dataset. In this study, three target features need to be balanced, as shown in Table III, which showcases examples of these target features, with each data sample representing a day's activities for an individual.

TABLE III
EXAMPLES OF TARGET FEATURES TO BE BALANCED

id	Activity Type	Chain Length	Duration (15-min)
1	{Home, Work, Home, Exercise, Home}	5	{28, 32, 4, 7, 6}
2	{Home, School, Buy meals, Home}	4	{25, 35, 8, 24}
3	Home, Work, Home	3	{30, 60, 15}

The proposed data balancing method iteratively calculates weights for each data sample based on its significance, then performs random resampling with replacement to produce a

Algorithm 1 Data balancing for multiple target features

Input: (1) Training dataset, (2) Adjustment rate at each step: $step_size$
Output: Weights W assigned to training dataset for data resampling

- 1: Select n target representation features and calculate the original distributions: $D_{ori} = \{O_1, O_2, \dots, O_n\}$
- 2: Ideal distribution for n target features: $D_{ideal} = \{I_1, I_2, \dots, I_n\}$
- 3: Initialize target distributions: $D_{tar} = \{T_1, T_2, \dots, T_n\} = D_{ori} = \{O_1, O_2, \dots, O_n\}$
- 4: **repeat**
- 5: **for** each feature i in n target features **do**
- 6: // Calculate the differences between adjusted and target share for each class in feature i :
- 7: $D_i = T_i - I_i$
- 8: \triangleright Adjust the elements based on its difference and the $step_size$:
- 9: $T_i = T_i - D_i \cdot step_size$
- 10: // Ensure the sum of percentages remains equal to 1 by normalizing the values:
- 11: $F_i = 1 / \sum(T_i)$ \triangleright define a normalization factor
- 12: $T_i = T_i \cdot F_i$ \triangleright update the target distribution
- 13: // Calculate weights for each sample (W) using the raking algorithm:
- 14: $W = raking(D_{ori}, D_{tar}, train_data)$
- 15: **end for**
- 16: **until** raking algorithm not converging or $|D_{tar} - D_{adj}| < threshold$
- 17: **return** W

balanced training dataset. This process can be summarized as in **Algorithm 1**, involving five key steps:

Step 1. Feature representation: As indicated in TABLE III, activity type and duration are recorded in sequence, while the length of activity chain is a singular value, making it difficult to balance. Therefore, the most frequently occurring activity type ("mode type") and activity duration ("mode duration") are selected from each activity chain, as representations of the original target features, excluding the first and last home activities, since most of activity chains start and end at home.

Step 2. Initial distribution D_{ori} computation: Calculate the real class distribution for each target feature.

Step 3. Target distribution D_{tar} specification: Set D_{tar} as an intermediate between the actual and ideal distributions D_{ideal} (uniform distribution) to facilitate convergence.

Step 4. Sample weights calculation: Compute sample weights to individual samples using the raking algorithm [48], based on D_{ori} and D_{tar} from **Steps 2** and **3**.

Step 5. Iterative refinement: If convergence is achieved, adjust D_{tar} closer to D_{ideal} and recalculate sample weights by repeating **Steps 3** and **4**.

D. Model Transfer

As aforementioned in Section I, modeling human mobility patterns in regions with limited data is challenging using traditional approaches. Even with advanced deep learning methods, such as transformer models, the data-hungry nature of these models can limit their effectiveness when datasets are small [46]. By leveraging the concept of transfer learning [49], we can address this challenge effectively. The proposed Deep Activity model, initially trained on the NHTS dataset (160,000 training samples), serves as a generic pre-trained model, which can then be fine-tuned using the limited local HTS data, adapting the generic model to the specific characteristics of smaller regions. The fine-tuning the Deep Activity model involves three primary steps:

Step 1: Adding new layers to adapt to new features. Augment the existing architecture with new layers to handle region-specific features and complexities, enabling better representation of diverse activity patterns.

Step 2: Freezing part of the pre-trained model. Initially freeze certain parts of the pre-trained NHTS model to maintain stability and leverage learned representations, preventing overfitting and ensuring effective capture of regional features.

Step 3: Fine-tuning with regional data and unfreezing layers. Train the modified model using regional datasets, updating weights of new layers. Gradually unfreeze selected parts of the pre-trained model, allowing comprehensive adaptation to unique regional patterns while retaining beneficial pre-trained knowledge.

The California and Puget Sound regions have input features similar to NHTS in terms of feature number, categories, and activity types. However, their datasets are relatively smaller (60,000 training samples for California and 8,000 for Puget Sound). For these regions, we apply only steps 2 and 3 of our process. In the case of Mexico City, which presents a distinct challenge due to its significantly reduced number of input features (40 compared to 60 in NHTS) and divergent activity types, we implement all three steps of our methodology.

E. Activity Location Assignment and Network Traffic Loading

To evaluate the Deep Activity model in a real-world transportation network and test its applicability for transportation system analysis, we propose an activity location assignment (ALA) method as an extension of the mobility pattern generation to enhance the model's functionality and ensure its practical application. This method aims to address the common limitation in travel survey data, where precise location information is often missing. The goal is to develop a simplified location assignment method for rapid implementation in regions without high-resolution location data.

The proposed method assigns zone-level locations Z for each predicted activity by considering the distribution of distances and angular deviations between preceding and subsequent activities. For large metropolitan regions, the spatial distribution is further refined by applying sub-region-specific distance and angle distributions to capture local spatial variations. This ensures that the assigned locations reflect the heterogeneity within different areas of the region. This is particularly important in large metropolitan areas, such as the Greater LA area, where spatial distributions may vary significantly across sub-regions, as shown in Fig. 4.

The proposed ALA process consists of the following key steps, as shown in **Algorithm 2**:

Step 1. Assigning TAZs for Mandatory Activities. The primary assumption is that each individual's home location is predetermined in the dataset. The first group of activities to be assigned locations are mandatory activities (e.g., work or school). For each individual, a home-to-work or home-to-school distance is assigned based on their demographic characteristics. Within each sub-region, these assigned distances follow the target distribution of commute distances between home and mandatory activity locations for that specific sub-region, denoted as D_{md} . A TAZ with the appropriate land

Algorithm 2 Activity Location Assignment

Input: (1) Fitted distributions for all sub-regions: home-work/school distance distribution $D_{md} = \{D_{md}^1, D_{md}^2, \dots, D_{md}^n\}$; Non-mandatory trip distance $D_{nmd} = \{D_{nmd}^1, D_{nmd}^2, \dots, D_{nmd}^n\}$; location angular difference distribution $D_{ad} = \{D_{ad}^1, D_{ad}^2, \dots, D_{ad}^n\}$; (2) Land use types of all zones LU ; (3) Zone-to-zone distance matrix M_d , angle matrix M_a ; (4) Home locations HL and predicted activity chains C for all agents.
Output: Assigned zone IDs $Z = \{Z^{md}, Z^{nmd}\}$ for all activities, including mandatory and non-mandatory activities.

```

1: repeat
2:   for each agent i with mandatory activities do
3:      $Dist_i = \text{sample}(D_{md})$   $\triangleright$  Assign home-work/school
      distance based on agent i's zonal distance distribution
4:      $Z_i^{md} = \text{match}(HL_i, Dist_i, LU)$   $\triangleright$  Select the most matched
      zone based on assigned distance from work/school zones and land use
      type
5:   end for
6:   for each non-mandatory trip j do
7:      $Dist_j = \text{sample}(D_{nmd})$   $\triangleright$  Assign distance to next zone
      based on last activity's zonal  $D_{nmd}$ 
8:      $Ang2Anc_j = \text{GetAngle}(M_a)$   $\triangleright$  Get the angle between
      previous zone and next anchor zone from angle matrix
9:      $AngD_j = \text{sample}(D_{ad})$   $\triangleright$  Assign angle difference based
      on last activity's zonal  $D_{ad}$ 
10:     $Ang_j = Ang2Anc_j + AngD_j$   $\triangleright$  Compute the direction to
      next location
11:     $Z_j^{nmd} = \text{match}(Dist_j, Ang_j, LU)$   $\triangleright$  Select the most
      matched zone based on the assigned distance, angle to next zone, and
      land use type
12:  end for
13:  Adjust the parameters of  $D_{md}$ ,  $D_{nmd}$ , and  $D_{ad}$  by a small
      margin to slightly change the shape of the distributions
14: until  $|N_{target} - N_{assigned}| < \text{threshold}$   $\triangleright$  Stop when
      the error of activity numbers across sub-regions between assigned and
      target locations is lower than threshold
15: return  $Z$ 

```

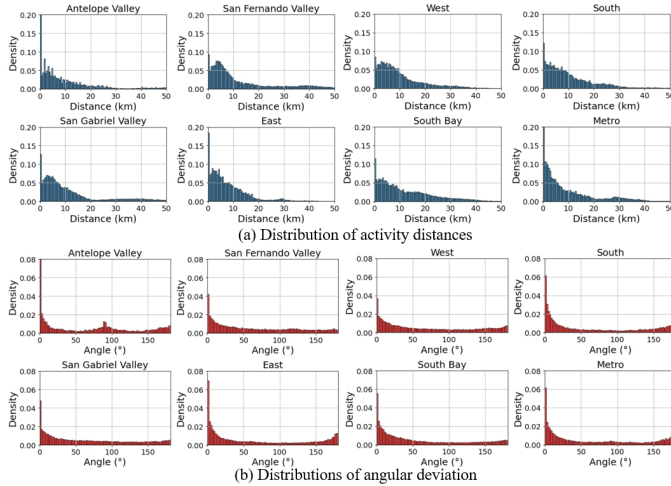


Fig. 4. Distributions of activity distances and angular deviations across sub-regions in LA

use type (work or school) and closely matching the assigned commute distance is then allocated to the individual.

Step 2. Assigning TAZs for Non-Mandatory Activities. After assigning TAZs for mandatory activities, these locations serve as anchor points within the individual's daily activity chain. The subsequent step involves assigning locations for non-mandatory activities (e.g., shopping, leisure, exercise) that occur between these anchor points. Non-mandatory activity locations are assigned based on two key parameters: (1) the distance to the next non-mandatory activity, and (2) the angular

deviation between the direct path to the next non-mandatory location and the direct path to the next anchor location. The assigned distances and angular deviations follow the target distributions of distance (D_{nmd}) and angular deviations (D_{ad}) for each sub-region, ensuring that the spatial distribution aligns with regional patterns.

Step 3. Refinement of Location Assignment. The objective of the location assignment process is to ensure that the spatial distribution of generated activity locations closely resembles the true activity distribution across sub-regions. This spatial similarity is assessed by comparing the occurrence frequencies of activities across sub-regions in the location assignment output with those in the ground truth data. To minimize bias in the generated distribution, the reference distributions used in Steps 1 and 2 are iteratively adjusted until the assigned activity number of sub-regions match the ground truth. This refinement process is initially applied to a small sample of the population to fine-tune the reference distributions for each sub-region. The refined distributions (D_{md} , D_{nmd} , and D_{ad}) are then applied to the larger population for large-scale transportation system analysis.

It is important to note that the objective of this location assignment method is not to predict the exact location of each activity, but rather to ensure a realistic spatial distribution of activity locations across the study area. This method provides a suitable input for subsequent transportation system analyses, such as regional traffic volume estimation and congestion assessment.

The mobility patterns and the corresponding activity location assignments together form a comprehensive regional travel demand input. This generated travel demand is integrated into an existing transportation simulation framework, LASim [50]. LASim is a large-scale, agent-based multimodal transportation simulation designed for the Greater LA area, as shown in Fig. 11 (c). The framework builds on the Multi-Agent Transport Simulation (MATSim) to tackle the challenges induced by urbanization and changing mobility patterns. By loading the synthesized travel demand into the LA roadway network, we can generate the synthetic traffic flow and further evaluate the transportation system performance based on the generated human mobility patterns.

VI. EXPERIMENTS AND RESULTS

A. Training and Evaluation Methods

All experiments are conducted on an NVIDIA RTX A5000 GPU. We employ the Adam optimizer with an initial learning rate of 0.005. The scheduler multiplicative decays the learning rate by a factor of 0.95 after each epoch. The model is trained on a dataset with 160,831 activity chains for training and 18,106 for validation over 150 epochs with a batch size of 512. To prevent overfitting, we use regularization methods like dropout and early stopping. Finally, a test set of 18,106 activity chains is used to evaluate performance.

Given the inherent uncertainty in human behavior, evaluating the accuracy of a specific agent can be challenging and may not always be appropriate. Therefore, the performance of the Deep Activity model is assessed at the system level by

comparing the similarity between the distributions of generated and real-world activity patterns, and the location assignment is evaluated at the traffic network level.

In this paper, the Jensen-Shannon Divergence (JSD) is used as the similarity metric [29], as shown in Equation 4. The goal is to minimize the difference between the distributions of generated and real activity patterns from activity chains. The metrics include: 1) **activity frequencies**, 2) **start times**, 3) **end times**, 4) **number of daily activities** (activity chain length), and 5) **duration of each activity**.

$$JSD(P||Q) = \frac{1}{2} \sum_{x \in X} \left[P(x) \log \left(\frac{P(x)}{M(x)} \right) \right] + \frac{1}{2} \sum_{x \in X} \left[Q(x) \log \left(\frac{Q(x)}{M(x)} \right) \right] \quad (4)$$

where $M = (P + Q)/2$. Here, P is the distribution of activity patterns from the generated activity chains, and Q is the distribution from the ground truth activity chains. X represents the full range of probabilities for a specific activity pattern statistic. A JSD value closer to zero indicates greater similarity between the distributions, showing the model's effectiveness in approximating the true distribution.

In addition to quantifying the model's performance at the distribution level using JSD values, it is also critical to analyze it at the chain level. By aggregating activity chains into graphs, where activity types are nodes and transitions between activities are edges, **completeness** of the activity chains, as the sixth metric, can be examined to ensure no activity types or transitions are missing. These graphs can be converted into transition matrices, which reveal the transition probabilities between any two pairs of activities. As the seventh metric, the **similarity of activity transition probability** is quantified by **Frobenius norm**, i.e., $|A - B|_F = \sqrt{\sum_{i=1}^m \sum_{j=1}^n |a_{ij} - b_{ij}|^2}$, where matrix A and B are the transition matrix of generated activity chains and the ground truth, respectively.

For the validation of the ALA and network traffic loading, given that the objective of the location assignment is not to precisely predict the next location in each activity chain, we do not employ metrics typically used in location prediction tasks, such as the accuracy of top-k recommended locations [51]. Instead, we compare the performance of the proposed method with SCAG ABM using transportation system-level metrics, including the cosine similarity of Origin-Destination Flow matrices [52], the number of activities across sub-regions [53], hourly vehicle-miles-traveled (VMT) [16], traffic volume [16], and traffic speed [16] over a 24-hour period. The error is quantified using Mean Absolute Percentage Errors (MAPE), a widely adopted measure in transportation system analysis [54]. We conduct performance evaluation at multiple scales, including network level and corridor level.

B. Baseline Models

Decoder-only transformer. In language modeling and sequence generation tasks, the "decoder-only transformer" is commonly adopted due to its effectiveness [55], making it a natural baseline for activity generation, allowing for a clear comparison when evaluating more complex models.

Recurrent Neural Network (RNN) and their variants are widely used for predicting travel behavior, e.g., next location prediction [56]. In this study, they are used as a comparison against the transformer-based models.

Vanilla RNN has a simple architecture where the output from the previous step is fed back into the network to influence the output of the current step [56].

Gated Recurrent Unit (GRU) introduces gating mechanisms to control the flow of information, maintain long-term dependencies, and address the vanishing gradient problem [57].

Long Short-Term Memory (LSTM) features a more complex architecture, consisting of three gates: the input gate, the forget gate, and the output gate [58], compared to the two gates used by GRU.

Large Language Models (LLMs) have demonstrated exceptional capabilities in understanding context and generating complex sequences without the need for extensive training periods, making them a suitable baseline for human mobility modeling. In our previous study [59], we utilized pre-trained models such as ChatGPT-4 and the open-source Llama2-70b to generate daily activity chains based solely on socio-demographic information, without the need for long-term training on domain-specific data.

C. Evaluation on Activity Generation

1) *Distribution Similarity:* To evaluate the performance of the proposed Deep Activity model, a comparative analysis is conducted involving the baseline models. The results of seven metrics are presented in Table IV, where the proposed Deep Activity model outperforms the others by achieving the lowest JSD values for activity chain length, duration, start time, and end time. These results indicate a high degree of similarity between the generated and ground truth activity patterns, underscoring the model's accuracy in capturing dynamic human activities. Additionally, it excels in edge completeness, with a percentage of 92.2%, significantly surpassing other models and illustrating its robustness in capturing the full spectrum of activity transitions. The LSTM model stands out in two metrics, showing superior performance compared to the Decoder-only Transformer. It achieves the lowest JSD value for activity type and the lowest Frobenius norm, indicating minimal discrepancy in transition probabilities between the generated and ground truth activity chains.

The LLMs demonstrate mixed results. While LLMs like GPT-4 show promise in activity type and chain length prediction, their higher JSD values for temporal aspects and lower edge completeness scores reveal significant limitations in capturing the complex dynamics of daily activities. These constraints, particularly evident in LLaMA2's underperformance across all metrics, indicate that current LLMs are not yet suitable for generating accurate activity chains without substantial adaptations to better model the nuanced patterns of human routines.

On the other hand, traditional models like GRU and RNN, with notably higher JSD values, demonstrate moderate performance but fall behind more advanced approaches. This

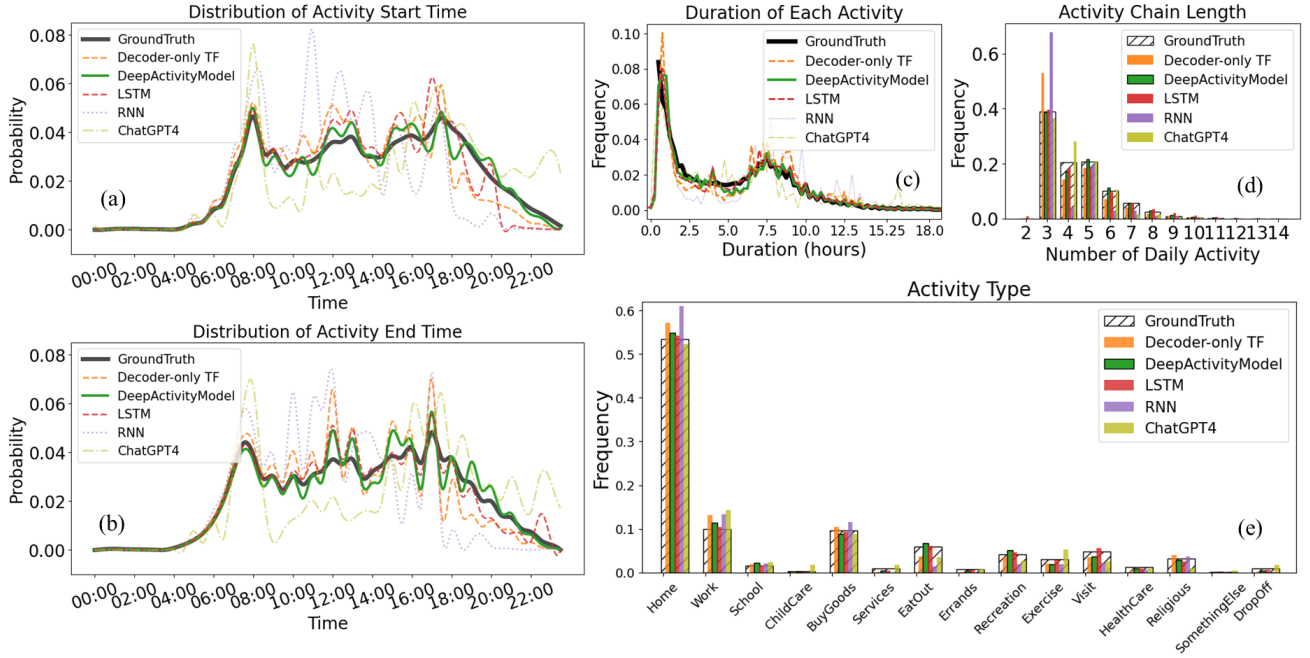


Fig. 5. Detailed analysis and comparison of activity generation on (a)(b) temporal dynamics, (c) activity chain length, (d) activity duration, and (e) activity type distribution.

indicates that they struggle to capture the complex temporal dependencies and transitions that characterize human activity patterns.

TABLE IV
ACTIVITY CHAIN GENERATION EVALUATION

Model	Len.	Dur.	Start	End	Type	EC	F-Norm
GRU	0.015	0.032	0.085	0.217	0.013	51.6%	0.934
RNN	0.064	0.029	0.067	0.121	0.024	50.9%	1.291
LSTM	0.006	0.003	0.019	0.004	0.003	91.4%	0.377
D-TF	0.011	0.011	0.014	0.012	0.013	67.1%	0.784
GPT-4	0.011	0.018	0.064	0.074	0.009	42.4%	1.111
LLaMA2	0.048	0.024	0.159	0.156	0.045	19.9%	1.404
Proposed	0.002	0.002	0.003	0.003	0.005	92.2%	0.643

*D-TF: decoder-only transformer; Len.: activity chain length; Dur.: duration of each activity; EC: edge completeness in percentage; F-Norm: Frobenius norm. All models reach 100% node (activity occurrence) completeness. Numbers except EC and F-Norm are JSD values.

In addition to the quantitative analysis, Fig. 5 provides a deeper insight into how each model performs in predicting specific details of human activities. Poorly performing models were excluded from the figure to maintain focus on the most relevant comparisons. For instance, in terms of start times (in Fig. 5(a)), both the LSTM and Decoder-only Transformer underestimate evening activities, whereas for end times (in Fig. 5(b)), the LSTM overestimates evening activities, and the Decoder-only Transformer overestimates midday activities. Meanwhile, ChatGPT4 demonstrates high volatility in predicting both start and end times, suggesting challenges in capturing consistent temporal patterns. Regarding the activity chain length (in Fig. 5(c)), the Decoder-only Transformer tends to generate three activities per day for individuals, while all models, except ChatGPT4, tend to underestimate the four-activity chains. This suggests a tendency in most models to

simplify daily activity sequences, potentially missing the complexity of real-world behavior. In terms of activity types (in Fig. 5(e)), Transformer-based models, LSTM, and ChatGPT4 perform well, especially for the common activities.

2) *Loss Term Ablation Study*: To assess the impact of individual loss terms in our Deep Activity model, we performed an ablation study, summarized in Table V. The findings illustrate how each loss term contributes to model performance across the seven metrics.

Removing the **soft label loss** (L_s) has the most significant impact across all metrics. This underscores the critical role of L_s in encouraging the model to explore different combinations and learn overall temporal patterns, rather than overfitting to specific time stamps. The flexibility provided by L_s appears crucial for capturing the inherent variability in human activity schedules. The absence of the **temporal order loss** (L_o) results in noticeable performance drops across all metrics, including duration and activity chain length. While the impact on start and end time predictions is less severe than removing L_s , the decline in length accuracy suggests that L_o plays a role in maintaining not just the chronological order, but also the overall structure of daily activity chains. When the **sequential timing loss** (L_{seq}) is removed, we observe relatively minor decreases in most metrics, with duration accuracy remaining largely unchanged. However, the higher Frobenius norm indicates that L_{seq} is particularly important for maintaining accurate activity transition probabilities, even if its impact on individual activity timings is less pronounced.

3) *Contextual Variation*: Distinct activity patterns between weekdays and weekends are effectively captured by the proposed model, as presented in Fig. 6. The start time distribution (a) reveals a later peak for weekend activities compared to weekdays, with a notable weekend shift towards midday

TABLE V
INFLUENCE OF EACH LOSS TERM

Loss	Len.	Dur.	Start	End	Type	EC	F-Norm
w/o L_s	.025	.012	.039	.024	.018	65.6%	.907
w/o L_o	.024	.011	.017	.016	.014	68.5%	.711
w/o L_{seq}	.013	.006	.015	.014	.013	72.6%	.739
All	.002	.002	.003	.003	.005	92.2%	.643

starts. In Fig. 6(b), there are more activities around 7.5 hours during weekdays, implying the working hours, which can also be reflected in Fig. 6(c). Clear variations are displayed in activity types, with work-related activities dominating weekdays while leisure activities like "EatOut" and "Visit" increase on weekends. Notably, the proposed model closely mirrors these temporal and categorical differences, demonstrating its ability to distinguish and reproduce weekday-weekend variations in human activity patterns.

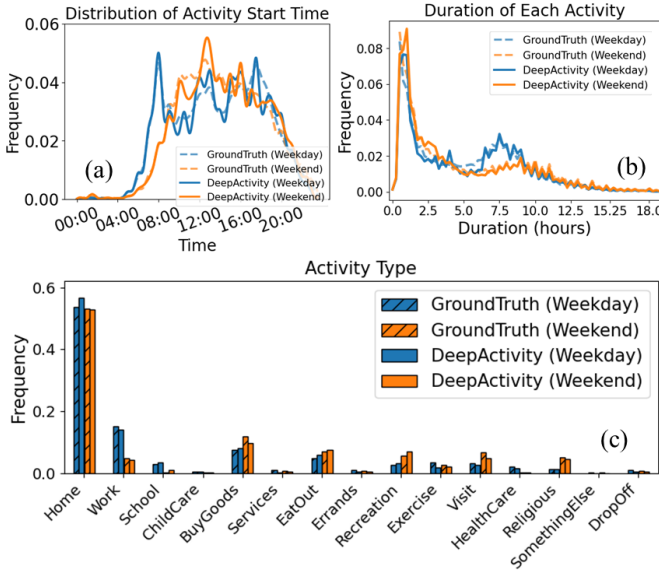


Fig. 6. Activity patterns in weekdays and weekends

Age is another crucial factor influencing activity patterns synthesis process, alongside day-of-week. Fig. 7 illustrates how the proposed model captures age-related differences across young (0-18), middle-aged (19-65), and elderly (65+) groups. In Fig. 7 (a), distinct end-time distributions are observed. Young individuals show peaks aligned with school schedules, middle-aged adults exhibit a more varied pattern reflecting diverse work commitments, while the elderly display a gradual curve peaking around midday. The activity type distribution in Fig. 7 (b) further highlights these differences, with high school attendance and recreation for the young, significant work-related activities for middle-aged, and increased shopping and eating time for the elderly. Notably, the Deep Activity model accurately reproduces these age-specific patterns in both timing and activity types, demonstrating its ability to synthesize realistic activity chains that reflect the distinct lifestyles associated with different age groups.

4) *Interdependency among Household members and Activity in Activity Generation*: The utilization of attention mech-

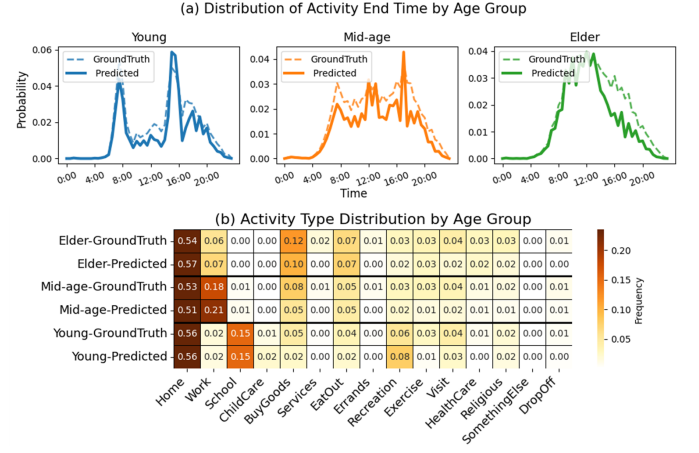


Fig. 7. Activity patterns across age groups

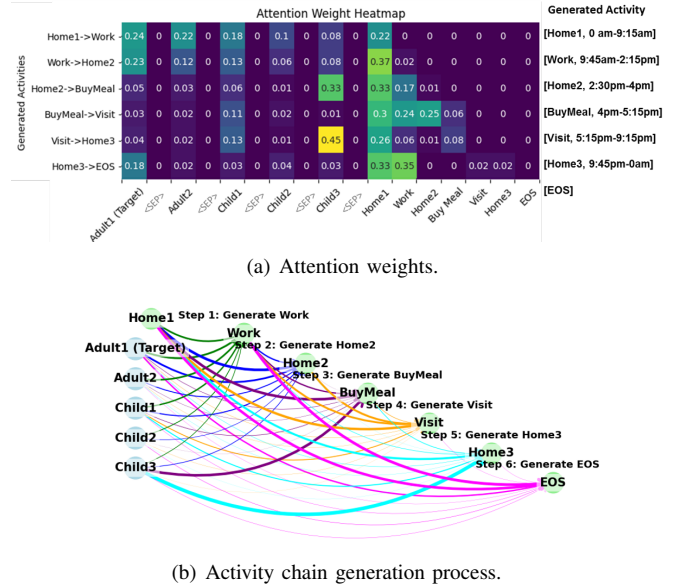


Fig. 8. Attention weights reveal the interdependency among household members and activities.

anisms in transformer models provides valuable insights into the decision-making processes within families, as illustrated by the detailed attention heatmap and graphical representation in Fig. 8. With its unique input data design, we are able to visit the attention from the first layer of encoder of the Deep Activity model, which reveals the interdependencies among the person's household and their activities.

Each row in the heat map (Fig. 8(a)) corresponds to specific activities of the target person—a male worker and father in a five-member family. The columns demonstrate how interactions with other family members and previous activities influence subsequent activities. The step-by-step activity generation is detailed in Fig. 8(b), where each step is labeled in a unique color, and the varied thickness of the lines indicates the relative influence of each interaction. For example, Child 3 exerts a significant influence on the target person's activities, such as "BuyMeal" and "Visit," highlighting the interdependencies of family members in coordinating daily schedules.

5) *Model Transferability*: To demonstrate the transferability of the proposed model, fine-tuning techniques are applied

to California, Puget Sound, and Mexico City. These regions cover diverse geographies and sizes, showing notable differences in mobility patterns (Fig. 9). Each dataset reveals distinct activity patterns in terms of timing, duration, type, and daily frequency.

For activity end times, Puget Sound and California peak around 17:00-18:00, while Mexico City shows three peaks, notably at 08:00 and 14:00-15:00. Puget Sound has more short activities (less than 0.5 hours) compared to the other regions. Chain lengths vary, with Mexico City having more 3-activity chains than other regions. "Home" is the most frequent activity type across all regions, followed by "Work." Mexico City has a higher proportion of "Home" and fewer "Work" activities than the U.S. regions. Activity types like "EatOut," "ChildCare," and "Visit" present in the U.S. datasets are missing from Mexico City HTS, where "Exercise" is grouped under "Recreation." These differences highlight challenges in standardizing activity classifications, emphasizing the need for region-specific fine-tuning of the NHTS pre-trained model to capture unique mobility behaviors.

Our fine-tuning approach has proven highly effective, as indicated in Table VI. The fine-tuned models have demonstrated the capability to transfer the generic model to different regions while maintaining robustness and achieving accuracy levels comparable to those obtained using the full NHTS dataset.

TABLE VI
TRANSFERRED DEEP ACTIVITY MODEL TO OTHER REGIONS

Region	Len.	Start	End	Dur.	Type	EC	F-Norm
California	.004	.013	.033	.002	.007	83.6%	.460
Puget Sound	.030	.009	.051	.010	.012	79.5%	.652
Mexico City	.010	.056	.010	.006	.009	63%	.339

To further illustrate the performance of our proposed method, we visualized detailed fine-tuning results for each region, as illustrated in Fig. 9. Importantly, although the transfer learning only uses very few samples, the model's predictions closely match the ground truth across all metrics and regions, with only minor discrepancies. This demonstrates the model's effectiveness in capturing and reproducing diverse regional mobility patterns, validating the success of the transfer learning approach in adapting to different urban environments.

6) *Data Balancing Algorithm Evaluation:* : Data balancing is performed on biased datasets to mitigate issues of skewed representation. To demonstrate its effectiveness, we focused on the most biased dataset in this study: the Mexico City dataset, specifically regarding activity length and activity type. The balancing process reduces the overrepresentation of common activities such as work and school, while enhancing the visibility of less frequent activities. It also reduced the dominance of 3-activity chains, helping to achieve a more even activity distribution. Importantly, while other features were adjusted, the overall activity duration distribution remained consistent. For better visualization, the dominant "Home" activity was excluded.

The outcomes of this balancing effort is elaborated in Fig. 10. Fig 10. (a) and (c) illustrate the adjusted distributions for activity type and length, with a noticeable reduction in

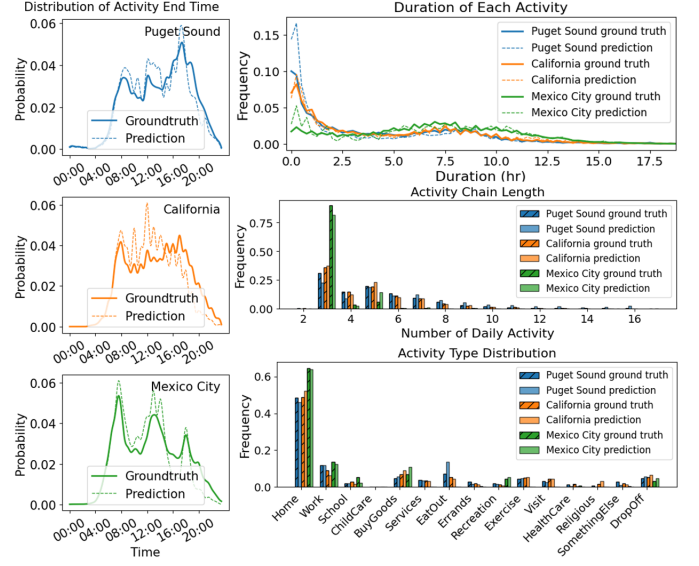


Fig. 9. Distribution comparison for datasets from three regions, showing significantly different activity patterns. Activity type labels are excluded because the dataset of Mexico City only contains 10 types of activity that are different from CA and Puget Sound region.

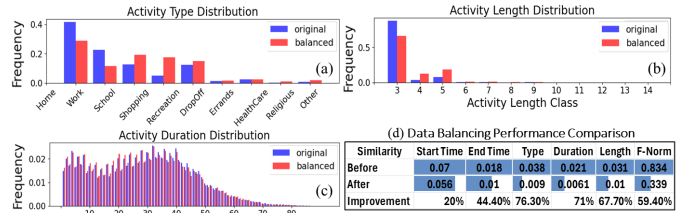


Fig. 10. Data balancing is performed on Mexico City.

overrepresented activities and chains. Fig10. (b) highlights that the activity duration distribution is preserved despite other changes. Fig 10. (d) depicts improvements in model performance metrics, showing significant reductions in JSD for activity type, from 0.038 to 0.009, indicating over 76.3% improvement. Frobenius Norm is also improved by 59.4%, from 0.834 to 0.339. Though temporal metrics show smaller enhancements due to the focus on activity duration, overall model performance benefits significantly from data balancing, demonstrating its effectiveness in mitigating dataset biases.

D. Validation of ALA and Network Traffic Loading

To validate the results of the ALA method and assess the transportation system-level performance of integrating the Deep Activity model with ALA in a large transportation network, we conduct a series of experiments. As shown in Fig. 11 (a), the LA County region is divided into eight sub-regions. We use 100,000 agents from the SCAG ABM dataset as a training set to transfer the mobility model initially trained on the NHTS dataset, and fine-tune the ALA to obtain reference distributions of distances and angles for each sub-region. The fine-tuned mobility generation model and ALA are then applied to a population sample of 1 million to evaluate its validity and scalability.

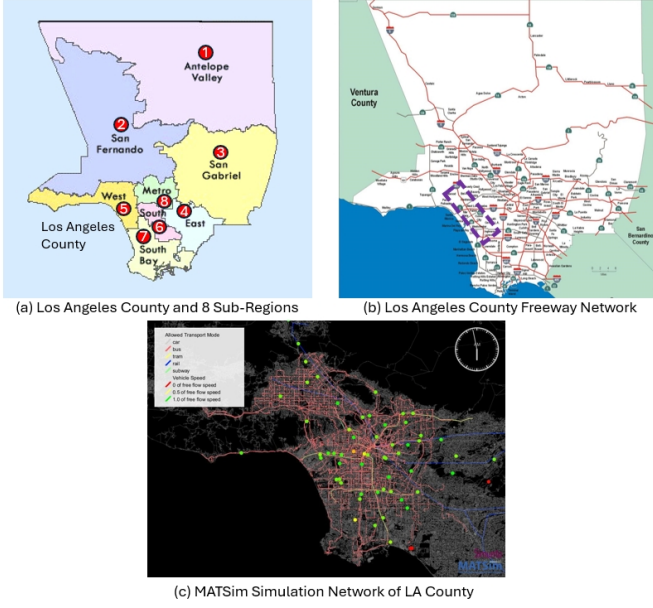


Fig. 11. LA County Map and Freeway Network.

Fig. 12 (a) presents the distribution of activity locations across sub-regions in LA County. The results demonstrate that the ALA effectively captures the spatial distribution of activity locations across all sub-regions. The cosine similarity of OD matrices between SCAG ABM and ALA is 0.997, indicating the flow pattern generated by ALA closely aligns with that of SCAG ABM. With the mobility patterns and assigned locations generated, we further load the travel demand into the LA transportation network, as depicted in Fig. 11 (b). The system-level traffic performance is illustrated in Fig. 12 (b), which shows the hourly VMT and traffic speed over 24 hours, aggregated across all freeway segments. From a network-wide perspective, the proposed Deep Activity model and ALA collectively ensure a well-aligned temporal distribution of traffic flow, yielding MAPEs of 4.97 for VMT and 1.16 for traffic speed when compared to benchmark results from SCAG ABM, demonstrating strong system-level performance.

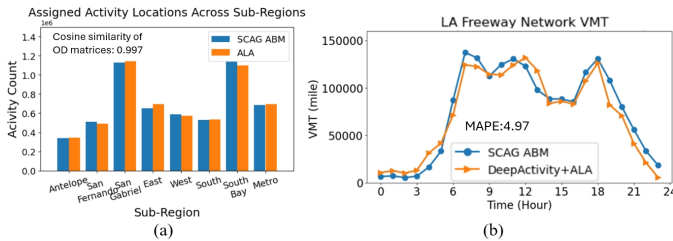


Fig. 12. Validation for ALA and traffic loading at network level.

Beyond the system-wide traffic metrics, we conduct further analysis at the corridor level by selecting a major segment from Interstate 405, a key freeway in the LA network. The location of the selected freeway segment is highlighted by the purple rectangle in Fig. 12 (b). The 24-hour traffic volume and speed in both directions on the target corridor segment are shown in Fig. 13 for comparison. To ensure the fidelity of the simulation, we include real-world observation data from the

Caltrans Performance Measurement System (PeMS) [60] as a reference and compare the results from our proposed model with those from the SCAG ABM data. Note that the MAPE is just calculated between the proposed model results and SCAG ABM, as PeMS data serve only as a reference. As seen

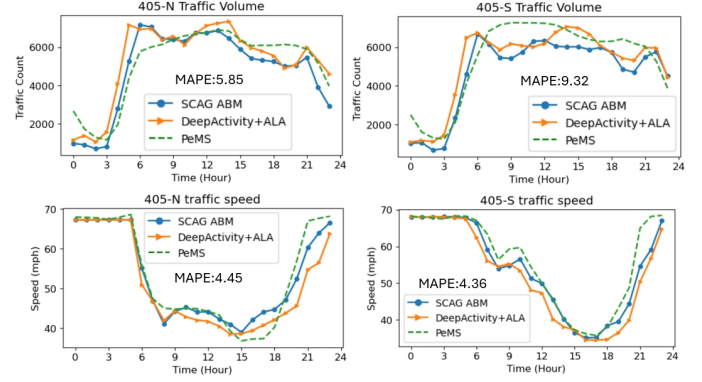


Fig. 13. Validation for ALA and traffic loading at corridor level.

in Fig. 13, PeMS observations indicate that both directions of the selected corridor experience high traffic volumes and significant congestion during the daytime. Notably, congestion patterns differ between the two directions: the northbound direction experiences major congestion throughout most of the midday, from 6 AM to 8 PM, while the southbound direction's primary congestion occurs after 12 PM and continues into the evening. The MAPE for traffic volume in the northbound and southbound directions is 5.85 and 9.32, respectively, while the MAPE for traffic speed in the northbound and southbound directions is 4.45 and 4.36, respectively.

These comparisons suggest that the proposed Deep Activity model and ALA successfully capture the dynamic temporal variations in traffic flow at the corridor level, demonstrating the model's good representation of the transportation system from both a travel demand generation and traffic loading perspective.

E. The Influence of Model Complexity and Data Size

The Deep Activity model was trained on the NHTS dataset, which has a modest sample size, potentially limiting the training effectiveness of complex models like Transformers. In this section, we explore the relationship between model complexity and data size in activity generation tasks.

To determine the optimal balance between model complexity and dataset size, we evaluated nine Transformer configurations on the NHTS dataset (180,000 samples). These models, which varied in the number of decoder layers (D), encoder layers (E), and attention heads (H), represented a spectrum of complexity, with parameters ranging from 434,000 to 2,344,000.

Our analysis, as illustrated in Fig. 14, indicated that models with fewer layers generally performed better, as reflected by lower JSD values and Frobenius norms. Simpler decoder-only models and those with a balanced encoder-decoder structure showed competitive results. Moreover, increasing the number of attention heads had only a moderate effect on performance.

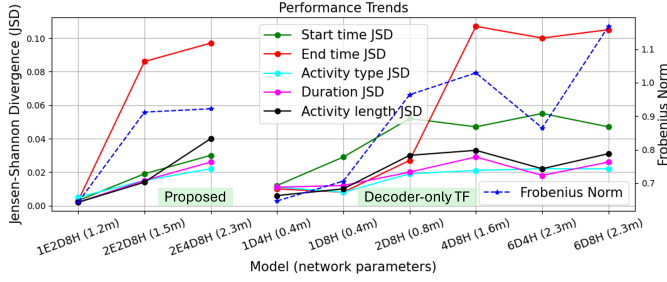


Fig. 14. Performance evaluation for transformer models with different complexity.

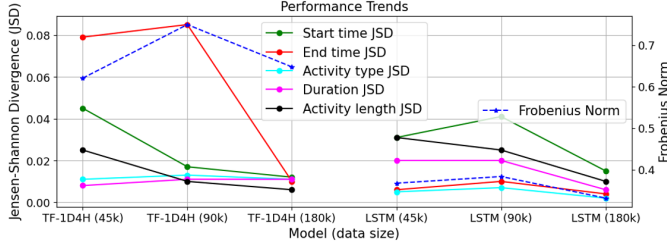


Fig. 15. Training data size effect on decoder-only transformer and LSTM.

This suggests that, for the given dataset size, adding more layers or attention heads does not guarantee improved performance and may lead to diminishing returns or increased complexity without significant accuracy gains.

To further understand the scaling effects of data size on different models, we compared a Transformer model with an LSTM model, as shown in Fig. 15. The Transformer exhibited improved performance with increased data size, from 45,000 to 180,000 samples, whereas the LSTM model's performance plateaued, indicating its limited ability to benefit from larger datasets. These results highlight the Transformer's superior capacity for utilizing larger datasets, aided by its parallel processing capabilities and global receptive field.

Model Selection. Given the modest sample size of the NHTS dataset, our findings suggest that: **1)** training on NHTS dataset, Transformer-based models with fewer layers perform better; **2)** the number of attention heads has moderate influence on the performance; **3)** Transformer-based model leverage larger datasets better, with performance increased when data size increases; **4)** LSTM-based models reach their limitation in current dataset and plateau with increased data size. Moreover, the explainability (as in Section VI-C4) and transferability (as in Section VI-C5) of transformer-based models resulted in choosing the transformer-based Deep Activity model.

VII. CONCLUSION AND FUTURE WORK

In this paper, we proposed the Deep Activity model, a generative deep learning approach for human mobility synthesis. We adopt the concept of "activity chains" to accurately represent the daily mobility patterns of individuals by applying household travel survey data in deep learning to model human mobility patterns, showcasing a pioneering method in the field. The Deep Activity model effectively generates realistic activity chains with high fidelity through a robust location assignment algorithm. Our experiments demonstrated

the model's versatility and robustness, achieving strong performance across various regions, including California, the Puget Sound area, and Mexico City. These results underscore the model's adaptability in generating diverse human mobility patterns, highlighting its potential for broader applications in urban planning and transportation analysis while maintaining a focus on data privacy.

Despite the achievements of the Deep Activity model, there are opportunities for future work. Our current approach is constrained by the limitations of existing HTS datasets, which often lack precise location data. As a result, our location assignment algorithm is currently limited to TAZ level trajectories. Enhancing the model with precise location data could improve accuracy and expand its applicability. However, current GPS datasets often lack semantic context (e.g., the type of activity). Addressing this gap through human trajectory data mining, as explored in our other study [61], could link semantic information with GPS data, enabling the creation of enriched datasets. Integrating location data at the POI level, combined with detailed activity and socio-demographic data, could enable more comprehensive modeling and yield deeper insights into human mobility patterns. These advancements would support more advanced applications in urban planning, transportation management, and policy-making.

ACKNOWLEDGMENTS

This study is supported by the Intelligence Advanced Research Projects Activity (IARPA) via Department of Interior/Interior Business Center (DOI/IBC) contract number 140D0423C0033. The U.S. Government is authorized to reproduce and distribute reprints for Governmental purposes notwithstanding any copyright annotation thereon. Disclaimer: The views and conclusions contained herein are those of the authors and should not be interpreted as necessarily representing the official policies or endorsements, either expressed or implied, of IARPA, DOI/IBC, or the U.S. Government.

REFERENCES

- [1] H. Ma, Y. Liu, Q. Jiang, B. Y. He, X. Liao, and J. Ma, "Mobility ai agents and networks," *IEEE Transactions on Intelligent Vehicles*, 2024.
- [2] D. Wang, B. Y. He, J. Gao, J. Y. Chow, K. Ozbay, and S. Iyer, "Impact of covid-19 behavioral inertia on reopening strategies for new york city transit," *International Journal of Transportation Science and Technology*, vol. 10, no. 2, pp. 197–211, 2021.
- [3] J. Zhang, B. Feng, Y. Wu, P. Xu, R. Ke, and N. Dong, "The effect of human mobility and control measures on traffic safety during covid-19 pandemic," *PLoS one*, vol. 16, no. 3, p. e0243263, 2021.
- [4] J. Hoppe, F. Schwinger, H. Haeger, J. Wernz, and M. Jarke, "Improving the prediction of passenger numbers in public transit networks by combining short-term forecasts with real-time occupancy data," *IEEE Open Journal of Intelligent Transportation Systems*, vol. 4, pp. 153–174, 2023.
- [5] M. U. Kraemer, C.-H. Yang, B. Gutierrez, C.-H. Wu, B. Klein, D. M. Pigott, O. C.-. D. W. Group†, L. Du Plessis, N. R. Faria, R. Li *et al.*, "The effect of human mobility and control measures on the covid-19 epidemic in china," *Science*, vol. 368, no. 6490, pp. 493–497, 2020.
- [6] H. Wu, L. Liu, Y. Yu, Z. Peng, H. Jiao, and Q. Niu, "An agent-based model simulation of human mobility based on mobile phone data: How commuting relates to congestion," *ISPRS International Journal of Geo-Information*, vol. 8, no. 7, p. 313, 2019.
- [7] D. I. Tselentis and E. Papadimitriou, "Driver profile and driving pattern recognition for road safety assessment: Main challenges and future directions," *IEEE Open Journal of Intelligent Transportation Systems*, vol. 4, pp. 83–100, 2023.

- [8] X. Liao, G. Wu, L. Yang, and M. J. Barth, "A real-world data-driven approach for estimating environmental impacts of traffic accidents," *Transportation research part D: transport and environment*, vol. 117, p. 103664, 2023.
- [9] L. Pappalardo, M. Vanhoof, L. Gabrielli, Z. Smoreda, D. Pedreschi, and F. Giannotti, "An analytical framework to nowcast well-being using mobile phone data," *International Journal of Data Science and Analytics*, vol. 2, pp. 75–92, 2016.
- [10] J. Abidi and F. Filali, "Mobility analytics of fans during the 2021 fifa arab cup tm football tournament in qatar," *IEEE Open Journal of Intelligent Transportation Systems*, 2023.
- [11] M. Bohm, M. Nanni, and L. Pappalardo, "Quantifying the presence of air pollutants over a road network in high spatio-temporal resolution," in *Climate Change AI, NeurIPS Workshop*, 2021.
- [12] N. Mohammadi and J. E. Taylor, "Urban energy flux: Spatiotemporal fluctuations of building energy consumption and human mobility-driven prediction," *Applied energy*, vol. 195, pp. 810–818, 2017.
- [13] M. E. Ben-Akiva and J. L. Bowman, "Activity based travel demand model systems," in *Equilibrium and advanced transportation modelling*. Springer, 1998, pp. 27–46.
- [14] M. Bradley and J. L. Bowman, "Design features of activity-based microsimulation models for us metropolitan planning organizations: a summary," in *Transportation Research Board Conference Proceedings*, vol. 2, no. 42, 2008.
- [15] B. Y. He, Q. Jiang, and J. Ma, "Connected automated vehicle impacts in southern california part-i: Travel behavior and demand analysis," *Transportation research part D: transport and environment*, vol. 109, p. 103329, 2022.
- [16] Q. Jiang, B. Y. He, and J. Ma, "Connected automated vehicle impacts in southern california part-ii: Vmt, emissions, and equity," *Transportation research part D: transport and environment*, vol. 109, p. 103381, 2022.
- [17] D. Karamshuk, C. Boldrini, M. Conti, and A. Passarella, "Human mobility models for opportunistic networks," *IEEE Communications Magazine*, vol. 49, no. 12, pp. 157–165, 2011.
- [18] M. Zhong, J. Kim, and Z. Zheng, "Estimating link flows in road networks with synthetic trajectory data generation: Inverse reinforcement learning approach," *IEEE Open Journal of Intelligent Transportation Systems*, vol. 4, pp. 14–29, 2023.
- [19] L. Pappalardo and F. Simini, "Data-driven generation of spatio-temporal routines in human mobility," *Data Mining and Knowledge Discovery*, vol. 32, no. 3, pp. 787–829, 2018.
- [20] Y. Zheng, Q. Wang, D. Zhuang, S. Wang, and J. Zhao, "Fairness-enhancing deep learning for ride-hailing demand prediction," *IEEE Open Journal of Intelligent Transportation Systems*, 2023.
- [21] M. C. Gonzalez, C. A. Hidalgo, and A.-L. Barabási, "Understanding individual human mobility patterns," *nature*, vol. 453, no. 7196, pp. 779–782, 2008.
- [22] L. Pappalardo, F. Simini, S. Rinzivillo, D. Pedreschi, F. Giannotti, and A.-L. Barabási, "Returners and explorers dichotomy in human mobility," *Nature communications*, vol. 6, no. 1, p. 8166, 2015.
- [23] S. Rinzivillo, L. Gabrielli, M. Nanni, L. Pappalardo, D. Pedreschi, and F. Giannotti, "The purpose of motion: Learning activities from individual mobility networks," in *2014 International conference on data science and advanced analytics (DSAA)*. IEEE, 2014, pp. 312–318.
- [24] C. M. Schneider, V. Belik, T. Couronné, Z. Smoreda, and M. C. González, "Unravelling daily human mobility motifs," *Journal of The Royal Society Interface*, vol. 10, no. 84, p. 20130246, 2013.
- [25] J. Cao, Q. Li, W. Tu, and F. Wang, "Characterizing preferred motif choices and distance impacts," *Plos one*, vol. 14, no. 4, p. e0215242, 2019.
- [26] T. Fontes, F. Murçós, E. Carneiro, J. Ribeiro, and R. J. Rossetti, "Leveraging social media as a source of mobility intelligence: An nlp-based approach," *IEEE Open Journal of Intelligent Transportation Systems*, 2023.
- [27] R. J. van Den Boogert and A. Y. Ding, "Engaging the crowd in sensing for smart mobility: A discrete choice experiment," *IEEE Open Journal of Intelligent Transportation Systems*, vol. 4, pp. 406–418, 2023.
- [28] N. McGuckin, A. Fucci *et al.*, "Summary of travel trends: 2017 national household travel survey," United States. Department of Transportation. Federal Highway Administration, Tech. Rep., 2018.
- [29] M. Luca, G. Barlacchi, B. Lepri, and L. Pappalardo, "A survey on deep learning for human mobility," *ACM Computing Surveys (CSUR)*, vol. 55, no. 1, pp. 1–44, 2021.
- [30] F. Zhou, Y. Dai, Q. Gao, P. Wang, and T. Zhong, "Self-supervised human mobility learning for next location prediction and trajectory classification," *Knowledge-Based Systems*, vol. 228, p. 107214, 2021.
- [31] C. Comito, "Next: A framework for next-place prediction on location based social networks," *Knowledge-Based Systems*, vol. 204, p. 106205, 2020.
- [32] J. Feng, Y. Li, C. Zhang, F. Sun, F. Meng, A. Guo, and D. Jin, "Deep-move: Predicting human mobility with attentional recurrent networks," in *Proceedings of the 2018 world wide web conference*, 2018, pp. 1459–1468.
- [33] J. L. Bowman and M. E. Ben-Akiva, "Activity-based disaggregate travel demand model system with activity schedules," *Transportation research part a: policy and practice*, vol. 35, no. 1, pp. 1–28, 2001.
- [34] K. G. Goulias, C. R. Bhat, R. M. Pendyala, Y. Chen, R. Paleti, K. C. Konduri, G. Huang, and H.-H. Hu, "Simulator of activities, greenhouse emissions, networks, and travel (simagent) in southern california: Design, implementation, preliminary findings, and integration plans," in *2011 IEEE Forum on Integrated and Sustainable Transportation Systems*. IEEE, 2011, pp. 164–169.
- [35] C. R. Bhat, K. G. Goulias, R. M. Pendyala, R. Paleti, R. Sidharthan, L. Schmitt, and H.-h. Hu, "A household-level activity pattern generation model for the simulator of activities, greenhouse emissions, networks, and travel (simagent) system in southern california," in *91st Annual Meeting of the Transportation Research Board, Washington, DC*, 2012.
- [36] C. Song, T. Koren, P. Wang, and A.-L. Barabási, "Modelling the scaling properties of human mobility," *Nature physics*, vol. 6, no. 10, pp. 818–823, 2010.
- [37] S. Jiang, Y. Yang, S. Gupta, D. Veneziano, S. Athavale, and M. C. González, "The timegeo modeling framework for urban mobility without travel surveys," *Proceedings of the National Academy of Sciences*, vol. 113, no. 37, pp. E5370–E5378, 2016.
- [38] S. Agriesti, V. Kuzmanovski, J. Hollmén, C. Roncoli, and B.-H. Nahmias-Biran, "A bayesian optimization approach for calibrating large-scale activity-based transport models," *IEEE Open Journal of Intelligent Transportation Systems*, 2023.
- [39] A. Kumar, S. Soni, S. Chauhan, S. Kaur, R. Sharma, P. Kalsi, R. Chauhan, and A. Birla, "Navigating the realm of generative models: Gans, diffusion, limitations, and future prospects—a review," in *International Conference on Cognitive Computing and Cyber Physical Systems*. Springer, 2023, pp. 301–319.
- [40] Federal Highway Administration, "2022 nextgen national household travel survey core data," U.S. Department of Transportation, Washington, DC, 2022.
- [41] New York Metropolitan Transportation Council, "2010-2011 regional household travel survey (rhts)," 2012, retrieved from: <https://www.nymtc.org/en-us/DATA-AND-MODELING/Travel-Surveys/2010-11-Travel-Survey>.
- [42] C. D. of Transportation, "California household travel survey," <https://www.nrel.gov/transportation/secure-transportation-data/tsdc-california-travel-survey.html>, 2012.
- [43] P. S. R. Council, "Puget sound regional council household travel survey," <https://www.nrel.gov/transportation/secure-transportation-data/tsdc-2017-puget-sound-travel-study.html>, 2017.
- [44] N. I. of Statistics and Geography, "Origin-destination survey in households of the metropolitan zone of the valley of mexico," <https://en.www.inegi.org.mx/programas/eod/2017/>, 2017.
- [45] Southern California Association of Governments (SCAG), "2016 Regional Travel Demand Model and Model Validation Report," Southern California Association of Governments, Tech. Rep., 2020.
- [46] A. Vaswani, N. Shazeer, N. Parmar, J. Uszkoreit, L. Jones, A. N. Gomez, Ł. Kaiser, and I. Polosukhin, "Attention is all you need," *Advances in neural information processing systems*, vol. 30, 2017.
- [47] A. Paszke, S. Gross, F. Massa, A. Lerer, J. Bradbury, G. Chanan, T. Killeen, Z. Lin, N. Gimelshein, L. Antiga *et al.*, "Pytorch: An imperative style, high-performance deep learning library," *Advances in neural information processing systems*, vol. 32, 2019.
- [48] J.-C. Deville, C.-E. Särndal, and O. Sautory, "Generalized raking procedures in survey sampling," *Journal of the American statistical Association*, vol. 88, no. 423, pp. 1013–1020, 1993.
- [49] F. Zhuang, Z. Qi, K. Duan, D. Xi, Y. Zhu, H. Zhu, H. Xiong, and Q. He, "A comprehensive survey on transfer learning," *Proceedings of the IEEE*, vol. 109, no. 1, pp. 43–76, 2020.
- [50] B. Y. He, Q. Jiang, M. Haoxuan, and J. Ma, "Multi-agent multimodal transportation simulation for mega-cities: Application of los angeles," *Procedia Computer Science*, vol. 238, pp. 736–741, 2024.
- [51] Q. Liu, S. Wu, L. Wang, and T. Tan, "Predicting the next location: A recurrent model with spatial and temporal contexts," in *Proceedings of the AAAI conference on artificial intelligence*, vol. 30, no. 1, 2016.

- [52] X. Guo, Z. Xu, J. Zhang, J. Lu, and H. Zhang, "An od flow clustering method based on vector constraints: a case study for beijing taxi origin-destination data," *ISPRS International Journal of Geo-Information*, vol. 9, no. 2, p. 128, 2020.
- [53] W. Mungthanya, S. Phithakkitnukoon, M. G. Demissie, L. Kattan, M. Veloso, C. Bento, and C. Ratti, "Constructing time-dependent origin-destination matrices with adaptive zoning scheme and measuring their similarities with taxi trajectory data," *IEEE Access*, vol. 7, pp. 77 723–77 737, 2019.
- [54] L. Li, X. Qu, J. Zhang, Y. Wang, and B. Ran, "Traffic speed prediction for intelligent transportation system based on a deep feature fusion model," *Journal of Intelligent Transportation Systems*, vol. 23, no. 6, pp. 605–616, 2019.
- [55] J. Roberts, "On the computational power of decoder-only transformer language models," *arXiv preprint arXiv:2305.17026*, 2023.
- [56] A. Al-Molegi, M. Jabreel, and B. Ghaleb, "Stf-rnn: Space time features-based recurrent neural network for predicting people next location," in *2016 IEEE Symposium Series on Computational Intelligence (SSCI)*. IEEE, 2016, pp. 1–7.
- [57] D. Liao, W. Liu, Y. Zhong, J. Li, and G. Wang, "Predicting activity and location with multi-task context aware recurrent neural network," in *IJCAI*, 2018, pp. 3435–3441.
- [58] K. Krishna, D. Jain, S. V. Mehta, and S. Choudhary, "An lstm based system for prediction of human activities with durations," *Proceedings of the ACM on Interactive, Mobile, Wearable and Ubiquitous Technologies*, vol. 1, no. 4, pp. 1–31, 2018.
- [59] Y. Liu, X. Liao, H. Ma, B. Y. He, C. Stanford, and J. Ma, "Human mobility modeling with limited information via large language models," *arXiv preprint arXiv:2409.17495*, 2024.
- [60] California Department of Transportation, "PeMS," 2020, retrieved from California Department of Transportation. [Online]. Available: <https://pems.dot.ca.gov>
- [61] Y. Liu, C. Kuai, H. Ma, X. Liao, B. Y. He, and J. Ma, "Semantic trajectory data mining with llm-informed poi classification," 2024.

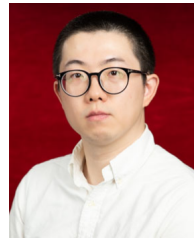


Xishun Liao received his Ph.D. degree in Electrical and Computer Engineering from the University of California, Riverside in 2023, the M.Eng. degree in Mechanical Engineering from the University of Maryland, College Park in 2018, and the B.E. degree in Mechanical Engineering and Automation from the Beijing University of Posts and Telecommunications in 2016. He is currently a research scientist at the University of California, Los Angeles. His research focuses include smart mobility systems, autonomous driving, human behavior modeling, applied AI/ML,

and digital twin.



Qinhua Jiang is a Ph.D. candidate from the Civil and Environmental Engineering Department, University of California, Los Angeles. He received his B.S. and M.S. degrees in civil engineering from Beijing Jiaotong University. His areas of expertise include activity-based travel demand modeling, AI/machine learning based traffic forecasting, and large-scale intelligent transportation system analysis.



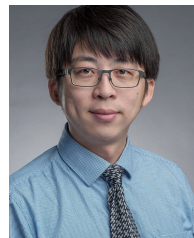
Yueshuai He received his Ph.D. in Transportation Planning and Engineering from New York University in 2020. Prior to his current role as an assistant professor at the University of Louisville, he was a research scientist at UCLA. He has extensive research experience in transportation system modeling, human mobility study, and sustainable mobility system planning and management. His work focuses on developing advanced statistical and computational simulation models to understand transportation system dynamics and facilitate the decision-making of public agencies. He obtained his Ph.D. in Transportation Planning and Engineering from New York University in 2020. Prior to his current role as an assistant professor at the University of Louisville, he was a research scientist at UCLA.



Yifan Liu is a Ph.D. student from the Civil and Environmental Engineering Department, University of California, Los Angeles. He received his M.S. degree in Computer Science from New York University in 2024 and his B.E. degree in Computer Science and Engineering from the University of California, Davis. His research interests include large language models, reinforcement learning, and deep learning, with a focus on applications to smart mobility systems and autonomous driving.



Chenchen Kuai received his M.S. in Transportation Engineering from the University of California, Los Angeles in 2024, and his B.S. in Highway and Bridge Engineering from Southeast University in 2022. He is currently pursuing a Ph.D. degree in the Zachary Department of Civil and Environmental Engineering at Texas A&M University. His research interests include Intelligent Transportation Systems, Complex Networks, Deep Learning, and Human Mobility.



Jiaqi Ma (Senior Member, IEEE) received the Ph.D. degree in transportation engineering from the University of Virginia, Charlottesville, VA, USA, in 2014. He is currently an Associate Professor with the Samueli School of Engineering, UCLA, where he is also the Faculty Lead of the New Mobility Program, Institute of Transportation Studies. His research interests include intelligent transportation systems, autonomous driving, and cooperative driving automation. He is a member of the TRB Standing Committee on Vehicle-Highway Automation, the

TRB Standing Committee on Artificial Intelligence and Advanced Computing Applications, and the American Society of Civil Engineers (ASCE) Connected and Autonomous Vehicles Impacts Committee. He is the Co-Chair of the IEEE ITS Society Technical Committee on Smart Mobility and Transportation 5.0. He is the Editor-in-Chief of the IEEE OPEN JOURNAL OF INTELLIGENT TRANSPORTATION SYSTEMS.